2018 IEEE International Conference on Soft Robotics (RoboSoft)
Livorno, Italy, April 24-28, 2018

Helical actuation on a soft inflated robot body

Laura H. Blumenschein, Nathan S. Usevitch, Brian H. Do, Elliot W. Hawkes, and Allison M. Okamura

Abstract— **Continuum and soft robots can leverage routed actuation schemes to take on useful shapes with few actuated degrees of freedom. The addition of vine-like growth to soft continuum robots opens up possibilities for creating deployable structures from compact packages and allowing manipulation and grasping of objects in cluttered or difficult-to-navigate environments. Helical shapes, with constant curvature and torsion, provide a starting point for the shapes and actuation strategies required for such applications. Building on the geometric and static solutions for continuum robot kinematics given constant curvature assumptions, we develop a static model of helical actuation and present the implementation and validation of this model. We also discuss the forces applied by the soft robot when wrapped around an object that deforms the static shape, allowing a quantification of grasping capabilities.**

I. Introduction

Compliance in soft or continuum robots allows them to take on a wide variety of shapes [1]. Continuum robots are often said to have "infinite" passive degrees of freedom, any of which can potentially be actuated. Designing actuators that leverage these continuous degrees of freedom in interesting ways enables numerous compelling behaviors and applications. However, in general, well-informed design of actuation strategies for soft robots requires knowledge of the relationship between the actuator design and the resulting kinematics. While some types of continuum robots have well described kinematics and dynamics, existing solutions cannot easily be extended to soft robots with compressible backbones.

In the design space for soft robot actuation, even very simple actuation strategies can lead to a wide range of behaviors, as can be seen in the design of generalized fiber-reinforced elastomeric actuators [2]–[5]. Many soft and continuum robots extend this approach to more degrees of freedom. These robots incorporate multiple actuated tendons into the surface of a long compliant body to shorten or lengthen surface paths and therefore cause the full structure to bend. In most designs, three straight actuators are used to control tip position, although some add a fourth tendon to allow for stiffness control [6]. The addition of helically routed tendons to straight tendons can increase the workspace and dexterity of the robot tip [7], [8].

Fig. 1. A soft, inflated robot is grown into a helical antenna. Shape is mechanically pre-programmed by pinching the thin walled plastic tube along a line of actuation. Growth is achieved by feeding more material through the center to be everted at the tip, and the material is flexible but not stretchable.

One type of continuum robot that has been recently developed is a soft inflatable robot that extends by growing like a plant (Fig. 1) [9], [10]. These robots rely on materials that are flexible but relatively inextensible (such as fabrics or thin plastic sheeting), meaning that deformation of the overall shape occurs by the material wrinkling, as opposed to material stretching. This robot grows by everting new material at the tip. Movement by growth allows for large length change of the robot and for the robot to access tight spaces or difficult to navigate environments. Previous work has examined the use of this growth to navigate an environment, needing only simple shape actuation to achieve movement in two or three dimensions [9]. The compact starting package for the robot relative to its final size lends itself to creating deployable structures [11]. Manipulation can be achieved by using the robot body as a grasper, an idea investigated in continuum robots imitating elephant trunks and octopus tentacles [12], [13]. The soft inflatable structure lends itself to creating the large shape changes needed for these applications. The use of inextensible materials means that shapes requiring large deformations can potentially be reached with less energy input than soft robots relying on extensible materials, because large amounts of elastic energy

This work was supported in part by National Science Foundation grant 1637446, Air Force Office of Scientific Research grant FA2386-17-1-4658, and the National Science Foundation Graduate Fellowship Program.

L. H. Blumenschein, N. S. Usevitch, B. H. Do, and A. M. Okamura are with the Department of Mechanical Engineering, Stanford University, Stanford, CA 94035 USA
(e-mail: lblumens@stanford.edu; usevitch@stanford.edu; brianhdo@stanford.edu; aokamura@stanford.edu).

E. W. Hawkes is with the Department of Mechanical Engineering, University of California, Santa Barbara, CA 93106 USA
(e-mail: ewhawkes@engineering.ucsb.edu).

need not be stored in the material.

Simple bending alone is not always the ideal actuation to achieve a shape for a desired application. One shape that could be effective in many applications is a uniform helix. Helical antennas, such as the prototype in Fig. 1, provide desirable operating characteristics and a deployable helical antenna is potentially useful in space exploration and search and rescue [14]. In addition, helical wrapping grasps can efficiently enclose objects leading to useful grasping mechanics for object acquisition and manipulation, as well as climbing [15]. To design actuators to achieve these desired shapes, we must develop the kinematics for helical actuation of soft inflated robots.

The large number of passive and active degrees of freedom in a continuum robot make traditional robotic kinematic and dynamic analysis difficult, even for uniformly routed helical actuators. As a result, this problem has been tackled at a variety of levels of complexity and accuracy. The most general solutions use Cosserat rod and Cosserat string theories to develop mechanics models of general tendon routings [16]. This model has been applied recently to helical actuation of a flexible backbone continuum robot [7]. However, these Cosserat-based models have been specifically developed for continuum robots with flexible backbones that are stiff in compression and require knowledge of material properties. Simpler models begin with geometrically constrained solutions. For the simplest tendon routings, i.e., straight tendons parallel to the backbone, the problem geometry results in piecewise-constant curvature sections, and this shape is a simple function of the tendon displacement [6]. This method of employing geometric constraints is translated easily to soft inflated robots. The importance of adding torsion to these models has been discussed [17] but has not yet been implemented in deriving the kinematics of a soft robot. In this work we derive the geometric constraints for helical actuation on a pneumatic soft robot and develop and validate a static kinematic model. This expands constant curvature kinematic models for continuum robots with the addition of constant, non-zero, torsion.

The remainder of the paper is organized as follows. Section II presents the geometric solution for helical actuation. This begins with discussion of the parameterization of the actuator and final achieved shape. We then define the geometric constraints used to relate the actuator to the robot shape and present the closed-form solution. Section III presents experimental results of the helical actuation, including prototypes implementing the described actuation, validation and discussion of the closed form solution, and measurements of forces applied by the soft robot when its shape is deformed.

II. Constant Curvature and Torsion Tendons

The piecewise constant curvature formulation of tendon actuated continuum robots can be extended for continuum robots where large torsion of the backbone is allowable. We focus the problem solution on an inflated tube robot, and a similar argument could be applied to other continuum robots.

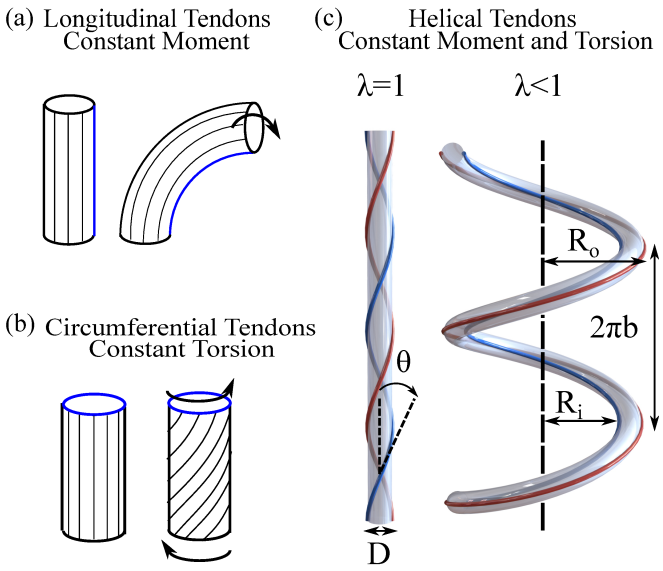

Fig. 2. Visualization of different types of uniform cable routings and their effect on robot shape, with the actuated cable shown in blue. In (a), contraction of a longitudinal cable creates a constant moment that leads to a constant curvature arc. In (b), pure torsion results from actuation of circumferential cables. In (c), the robot with helical cables is shown in both unactuated and actuated states. The actuator is shown with the blue line and the diametrically opposite line is in red. The actuator parameters, θ, D, λ, and shape parameters, R_o, R_i, b, are displayed.

To develop this geometric model, we define the problem, including the actuator parameterization and geometric constraints, and then present the closed-form solution.

A. Shape Model

1) Geometric Model of Actuator Shape with Helical Tendons: To achieve a uniform deformed shape, the continuum robot actuator must route in a uniform path on the surface of the body. Uniform tendons may be routed on the robot's surface axially, circumferentially, and at an intermediate angle. The traditional routing of tendons on a continuum robot in a straight path parallel to the undeformed backbone leads to constant-curvature, zero-torsion deformation when actuated (Fig. 2a) . A circumferential routing of an actuator, if realizable, would lead to pure torsion of the backbone (Fig. 2b). Helical tendon routing is a mixture of these two extremes and leads to both curvature and torsion of the backbone when actuated (Fig. 2c).

We will quantify the relationship between the helical path of an actuator around an undeformed pneumatic tube and the resulting helical shape of the actuated pneumatic tube. To develop this relationship, we first give the standard parameterization of a helix in terms of its radius and pitch,

$$r(s) = \begin{bmatrix} R\sin(s) \\ R\cos(s) \\ b\,s \end{bmatrix} \tag{1}$$

where R is the radius of a helical path and b is the normalized pitch parameter such that $2\pi b$ is the height achieved by one revolution of the helix. The actuator must lie on the body of the robot, so the actuator radius is equal to the thin-walled

tube radius. In our parameterization of the helical actuator path around the tube we use variations of these standard parameters. For the intuitiveness of our formulation and to allow our model to cover the straight actuator case as well, it is convenient to use the tube diameter, D, in place of the radius and to replace the pitch, b, with the angle of the path with respect to the straight actuator, θ, which is defined as

$$\theta = \arctan \frac{D}{2b_a} \tag{2}$$

where D is the diameter of the tube, and b_a is the normalized pitch of the actuator about the undeformed tube.

These parameters define the path of the uncontracted actuator. A third parameter is necessary to describe the amount of actuation along the helical path. For a purely geometric model, we parameterize the actuation using the relative shortening of the path length when actuated compared to the path length when not actuated. We use λ to represent this ratio. Figure 2c shows the parameters used to describe the actuator shape on the initial tube and the parameters of the resulting helix after actuation discussed in the subsequent section.

2) Resulting Helical Shape: Because the helical actuator path is uniform and generates both curvature and torsion in the soft robot backbone, the resulting backbone path will have constant curvature and constant torsion. A path with both of these properties is a helix.

To understand the resulting shape further, we observe how the soft pneumatic beam robot deforms to achieve the final shape. The pneumatic beam is made of inextensible plastic or fabric so it can only shorten to change shape, not lengthen. It accomplishes this length change by wrinkling the thin wall of the material at discrete locations. While a tip load will only cause one or a few buckle points to occur in the body, the distributed loading caused by a body-embedded tendon causes distributed wrinkling that approximates a continuous shortening along the path of the actuator. The maximum wrinkling will occur at the location of the actuator, and no wrinkling will occur diametrically opposite to the point of highest wrinkling.

We define the robot shape by parameterizing the actuator path $r_i(s)$ (the path with the highest wrinkling) and the path diametrically opposite the actuator $r_o(s)$ (the path with no wrinkling) with a common parameter s (Fig. 3) as follows:

$$\vec{r}_i(s) = \begin{bmatrix} R_i \sin(s) & R_i \cos(s) & b\, s \end{bmatrix}^T \tag{3}$$

$$\vec{r}_o(s) = \begin{bmatrix} R_o \sin(s) & R_o \cos(s) & b\, s \end{bmatrix}^T \tag{4}$$

where R_i is the radius of the inner helix, R_o is the radius of the outer helix, and b is the normalized pitch of the helices.

In addition to the actuator paths, we can also define the center path of the robot as:

$$\vec{r}_c(s) = \frac{1}{2}(\vec{r}_i(s) + \vec{r}_o(s)). \tag{5}$$

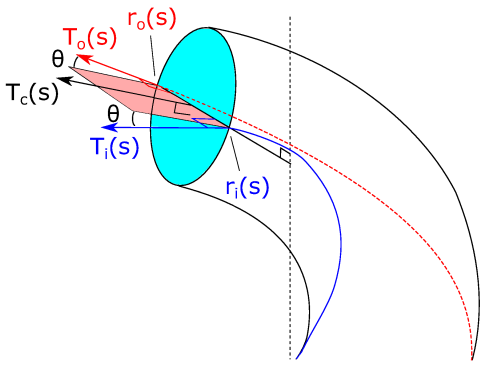

Fig. 3. Diagram of the geometric relationships between the actuator path (blue) and the diametrically opposite path (red). The two paths are parameterized by s. The points $r_o(s)$ and $r_i(s)$ are separated by a distance D. The tangent vectors to these curves ($T_o(s)$ and $T_i(s)$) are orthogonal to $r_o(s) - r_i(s)$. The angle between each tangent vector and the center tangent ($T_c(s)$) is θ, giving a total of 2θ between the inner and outer tangent vectors. The blue circular cross section is normal to the center tangent vector $T_c(s)$.

3) Geometric Constraints: The relationship between the parameters defining the spiraling path around the unactuated tube and actuation state of the actuators (θ,D,λ) and the parameters defining the final shape of an actuated helix (R_o,R_i,b) are developed through an understanding of the geometric constraints imposed by the tube material. We define constraints to relate properties of the shortest and longest helical paths to each other with the actuator parameters.

Looking at the full paths, we know that the ratio of the outer arc length and inner arc length over any portion of the robot should be equal to the contraction ratio. For the helices described in Eq. 3 and 4, and looking at the interval $s \in [0, S]$, this constraint can be written:

$$\lambda = \frac{\sqrt{(Sb)^2 + (SR_i)^2}}{\sqrt{(Sb)^2 + (SR_o)^2}} = \frac{\sqrt{b^2 + R_i^2}}{\sqrt{b^2 + R_o^2}} \tag{6}$$

This constraint is defined by how much the inner path is shortened relative to the outer, unwrinkled, path.

The remaining constraints define the relationship between the inner and outer paths for any points $r_i(s)$ and $r_o(s)$ for a common value s along the robot. These constraints are portrayed graphically in Fig. 3. When the tube is under pressure, the restriction imposed by the tube is that disks normal to the backbone $r_c(s)$ $(s \in [0, S])$ are circles of diameter D. As the tube wrinkles, these cross-sections move relative to one another but remain approximately circular. This circular shape imposes the constraint that the distance between two points $r_o(s)$ and $r_i(s)$ is the tube diameter, which in terms of the parameters can be expressed:

$$D = R_o - R_i \tag{7}$$

The final constraint is that the angle between each tangent vector and the center line is θ. This follows from the observation that the tangent vectors to the inner, outer, and center curves ($\vec{T}_i(s)$, $\vec{T}_o(s)$ and $\vec{T}_c(s)$) are all normal to $(r_o(s) - r_i(s))$, and that $(r_o(s) - r_i(s))$ is normal to the

TABLE I

SUMMARY OF THE FORWARD AND INVERSE STATIC SOLUTIONS OF HELICAL ACTUATION

Inverse Solution	Radius and Pitch Parameterized Forward Solution	Curvature and Torsion Parameterized Forward Solution
$\lambda = \frac{\sqrt{b^2+R_i^2}}{\sqrt{b^2+R_o^2}} \quad D = R_o - R_i$	$R_o = \frac{D(1-\lambda\cos(2\theta))}{1+\lambda^2-2\lambda\cos(2\theta)} \quad R_i = \frac{D\lambda(\cos(2\theta)-\lambda)}{1+\lambda^2-2\lambda\cos(2\theta)}$	$\kappa_o = \frac{1-\lambda\cos(2\theta)}{D} \quad \tau_o = \frac{\lambda\sin(2\theta)}{D}$
$\theta = \frac{1}{2}\arccos(\frac{R_iR_o+b^2}{\sqrt{b^2+R_i^2}\sqrt{b^2+R_o^2}})$	$b = \frac{D\lambda\sin(2\theta)}{1+\lambda^2-2\lambda\cos(2\theta)}$	$\kappa_i = \frac{\cos(2\theta)-\lambda}{D\lambda} \quad \tau_i = \frac{\sin(2\theta)}{D\lambda}$

center axis about which the helices spirals. This is equivalent to saying that the angle between $\vec{T}_i(s)$ and $\vec{T}_o(s)$ is 2θ.

This constraint can also be viewed in terms of the normal and tangent vectors obtained from a Frenet-Serret frame of the parameterization in (1):

$$T(s) = \frac{\dot{r}(s)}{\|\dot{r}(s)\|} = \frac{1}{\sqrt{b^2+R^2}} \begin{bmatrix} R\cos(s) \\ -R\sin(s) \\ b \end{bmatrix} \tag{8}$$

$$N(s) = \frac{\dot{T}(s)}{\|\dot{T}(s)\|} = \begin{bmatrix} -\sin(s) \\ -\cos(s) \\ 0 \end{bmatrix} \tag{9}$$

where $T(s)$ is the unit tangent vector and $N(s)$ is the unit normal vector to the curve. Using the Frenet-Serret frame representation, the normal vector to a helical path lies in the xy plane and in the same direction for both paths. Since the normal vectors are aligned, the tangent vectors for each path can only differ by a simple rotation about the common normal vector. We defined the angle between the actuator path and the center body path in (2) as θ, and, since the inner and outer paths are identical before actuation, the total angle between the tangent vectors will be 2θ. This relationship is diagrammed in Fig. 3. We can capture this relationship with the dot product of the tangent vectors:

$$\vec{T}_i^T\vec{T}_o = \|\vec{T}_i\|\|\vec{T}_o\|\cos(2\theta) = \cos(2\theta) \tag{10}$$

Substituting in the tangent vector from (8) we get the final constraint:

$$\cos(2\theta) = \frac{R_iR_o + b^2}{\sqrt{b^2+R_i^2}\sqrt{b^2+R_o^2}} \tag{11}$$

B. Closed-Form Solution

The three geometric constraints in (6), (7), and (11) define the relationship between the actuator parameterization and the robot shape parameterization. In fact, the equations in their current form give a solution for the inverse problem, taking the desired robot helical shape and giving the actuator shape to achieve it. A forward solution can be solved from the equations as:

$$\begin{aligned} R_o &= \frac{D(1-\lambda\cos(2\theta))}{1+\lambda^2-2\lambda\cos(2\theta)} \\ R_i &= \frac{D\lambda(\cos(2\theta)-\lambda)}{1+\lambda^2-2\lambda\cos(2\theta)} \\ b &= \frac{D\lambda\sin(2\theta)}{1+\lambda^2-2\lambda\cos(2\theta)} \end{aligned} \tag{12}$$

With these equations we can calculate the resulting helical shape from an actuator configuration. These equations can be reformulated in terms of curvature and torsion to get additional insight, using the following substitution:

$$\kappa = \frac{R}{b^2+R^2} \qquad \tau = \frac{b}{b^2+R^2} \tag{13}$$

where κ is the helix curvature and τ is the helix torsion. With this substitution, there are now four parameters describing the robot body shape (κ_o, κ_i, τ_o, and τ_i) but still only three equations. This can be remedied by adding the implied constraint that was assumed by setting the inner and outer pitch equal when developing the robot body parameterization:

$$b = b_o = b_i \Rightarrow \frac{\tau_o}{\tau_o^2+\kappa_o^2} = \frac{\tau_i}{\tau_i^2+\kappa_i^2} \tag{14}$$

Substituting the solutions in (12) into the variable re-parameterization in (13) gives:

$$\begin{aligned} \kappa_o &= \frac{1-\lambda\cos(2\theta)}{D} & \tau_o &= \frac{\lambda\sin(2\theta)}{D} \\ \kappa_i &= \frac{\cos(2\theta)-\lambda}{D\lambda} & \tau_i &= \frac{\sin(2\theta)}{D\lambda} \end{aligned} \tag{15}$$

The forward and inverse solutions for the constant curvature, constant torsion actuation are summarized in Table I.

III. EXPERIMENTAL RESULTS

The geometric mapping developed in the analysis of constant curvature and torsion actuation on a soft inflated body was tested against physical prototypes to determine the validity of the model. We begin by discussing three different actuation methods with helical paths implemented on our robot body. We then present validation of the developed model using one of the described implementations and discuss implications of the model equations. This is followed by experiments showing the deformations of the static shapes under radial and axial loading of the helix.

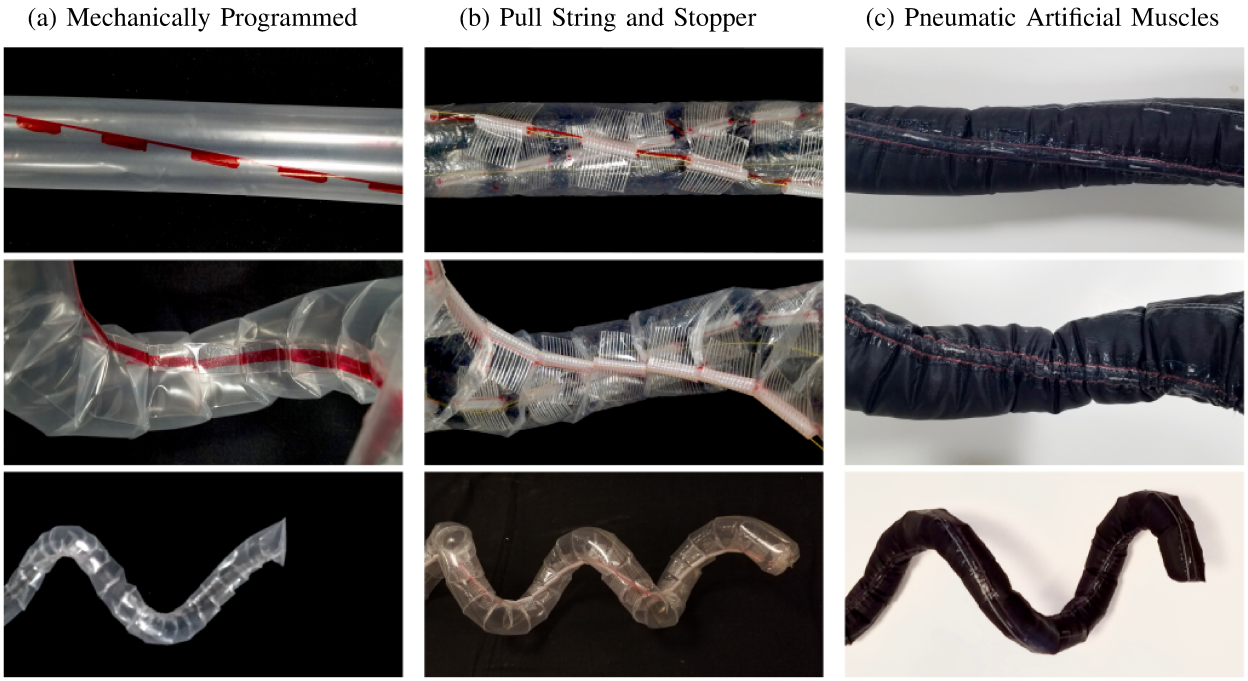

Fig. 4. Implementation of helix actuation. (a) Mechanically programmed implementation uses discrete removal of material using tape along line of actuation to achieve a single static shape that can be grown. (b) Pull string and stopper implementation creates one shape when the string is fully relaxed and another when the stoppers are fully connected, allowing actuation between two shapes. (c) IPAM implementation [18] allows for approximately continuous change of λ during actuation. Material wrinkles along the full line of actuation to reduce length.

A. Implementation

We implemented the helical actuation of our soft inflated robot body using three different methods, as shown in Fig. 4. These methods allow different amounts of control of the shape, from growth into a single set shape to actuation among a range of helical shapes.

1) Mechanically Programmed: The first implementation we refer to as being mechanically programmed, meaning that the shape is pre-determined by the manufacturing process. The robot body can then be grown into this predetermined shape. In tasks where the desired path is known or can be planned ahead of time this implementation allows precise shape control. Despite this implementation not being "actuated" in the sense that it changes shape actively, we can use the same ideas of actuator routing and shortening of the actuator path to describe the permanent shapes achieved.

The robot body is mechanically programmed by removing discrete sections of material along a length. These sections are pinched together and held by tape. The tape pieces are narrow to approximate a wrinkle in the material cross-section that is maximized at the line of actuation. Though the actual description of the model describes a proportional shortening along the entire length of actuation, this can be well approximated by alternating pinched and straight sections at a sufficiently tight spacing, as seen in Fig. 4a.

2) Pull String and Stoppers: The second implementation can be used to actuate between two shapes, usually a straight tube and a desired helical shape. This is done by arranging alternating gaps and stoppers along the line of actuation (Fig. 4b). A pull cable is fed through the stoppers and attached to the far end of the robot. When this string is pulled, the gaps collapse along the line of actuation and only the stoppers are left. This is similar to the mechanically programmed implementation, in which discrete sections are fully wrinkled and the remaining material is left extended. The value of λ will be the ratio between the stopper length and the stopper and gap length together.

We created this actuation using PTFE tubing for the stoppers and high molecular weight polyethylene braided line for the pull cable. This combination provided a low coefficient of friction, which is beneficial since the force needed to pull the cable will increase as the helical path is formed [19]. The pull cable implementation can only be used to actuate between two discrete shapes because a uniform value for λ along the line of actuation will not be guaranteed until the cable is fully actuated and all the stoppers are touching. In practice, this happens because, as the cable is actuated, the tube will buckle first at a single point. This buckled point will have a much lower stiffness than the unbuckled tube and so will continue to be the location of bending until the stoppers touch. Then a new buckling point will appear. This will repeat until all the stoppers are touching, at which point uniform actuation can be guaranteed.

3) Pneumatic Artificial Muscles: Pneumatic muscles are a class of actuators that change length or shape based on the internal pressure in the actuator [18], [20], [21]. When made uniformly, the muscles will have uniform contraction or expansion along the length.

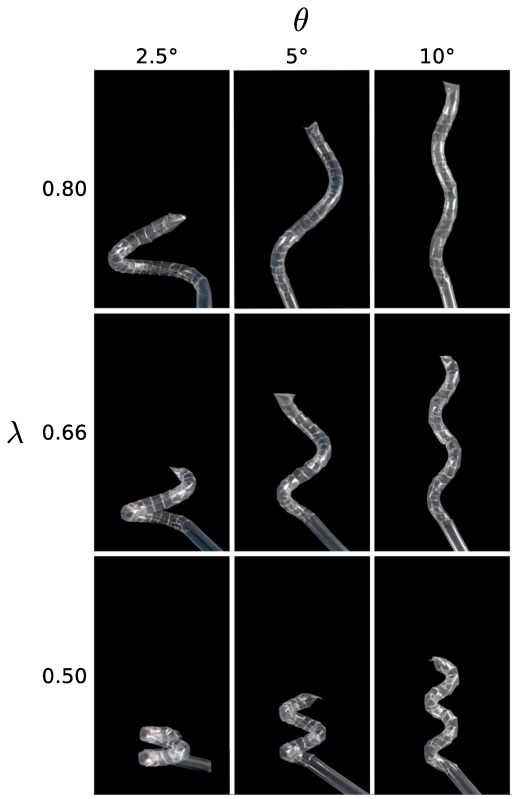

Fig. 5. Helix prototypes varying λ and θ. Helix tightens as λ is decreased and θ changes the ratio between the pitch and the radius.

For our final implementation we used inverse pneumatic artificial muscles (IPAMs). These pneumatically powered actuators extend uniformly as the internal pressure is increased and can be constructed for high stroke [18]. Constructing a robot with an IPAM along the line of actuation, we can achieve an implementation that can continuously change λ value within a range with a set θ and D (Fig. 4c). Unlike the mechanically programmed and pull cable implementations, the value of λ is not inherently known from the construction, so either a mapping must be developed to relate the pressure to the shape or another measurement of the actuator strain will be needed.

B. Shape Model Validation

The static solution developed in Section II was tested by creating actuated helical shapes while varying λ and θ. To quickly and easily create desired test shapes with a range of parameters, we used mechanically programmed implementation described in Section III-A.1. Values for θ were $2.5°$, $5°$,and $10°$, and values of λ were between 0.9 and 0.5. The tube diameter, D, was held constant for the test shapes at 3.31 cm. A selection of the resulting test helices can be seen displayed in a grid format in Fig. 5. For a one-to-one comparison, the constructed helices all started with the same initial tube length. Qualitatively, changes in θ changed the relationship between the pitch and radius of the path, modifying the slope of the helix, while changes in λ tightened or loosened the helix.

Fig. 6. Scaling up D by 2.5 times and holding λ and θ constant leads to direct scaling of final shape parameters by 2.5 times as expected.

Diameter variation was not needed because the equations for R_o, R_i, and b of the resulting helical shape are all proportional to D as seen in Table I. So the expected effect of changing D is a direct scaling of the resulting shape, given the same λ and θ. This was verified for a single case of the test shapes, constructing a helical actuation with the diameter increased by 2.5 times and with θ equal to $5°$ and λ equal to 0.66 (Fig. 6). The resulting larger helix had the same shape as the original helix but with radii and pitch scaled up by 2.5 times.

The shape of a test helix was measured by identifying a single rotation of the helix and then measuring the inside and outside arc lengths. This measurement technique assumed that the test helices have a uniform shape, which was verified visually. The helix parameters could be found from the arc lengths and tube diameter by the relationship:

$$R_o = \frac{L_o^2 - L_i^2}{8\pi^2 D} - \frac{D}{2} \qquad R_i = \frac{L_o^2 - L_i^2}{8\pi^2 D} - \frac{3D}{2}$$
$$b = \sqrt{\frac{L_o^2}{4\pi^2} - R_o^2} \tag{16}$$

where L_o is the outer arc length and L_i is the inner arc length of the helix. These equations are derived from the arc length calculation for uniform helices, which for a single revolution is:

$$L = \sqrt{(2\pi R)^2 + (2\pi b)^2} \tag{17}$$

We can solve for the parameters, R_o, R_i, and b, with the addition of the diameter constraint in (7). For shapes that did not make a full rotation in the given length, a half rotation arc length was measured and doubled. The parameter measurements of the test helices were compared to the parameters predicted by the equations in Table I and the results for R_o and b are plotted in Fig. 7. The data from the test helices matched the predicted relationships well with an average error of 2.6 mm for the outer radius and 3.3 mm for the pitch parameter.

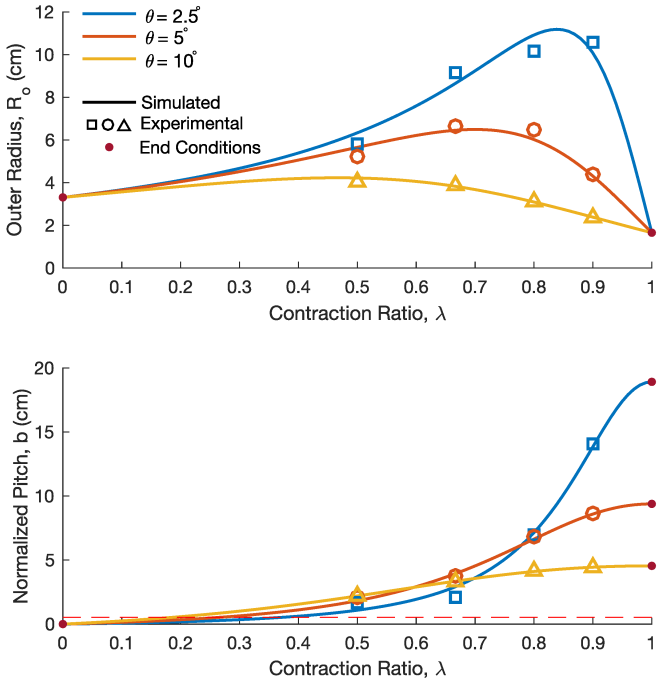

Fig. 7. Comparison of the model to test helices. Model is shown for the full contraction range, λ, and for three values of actuator angle, θ. All tests were done with a tube diameter, D, of 3.31 cm. Values of pitch below the dotted red line are not realizable as the robot will self-intersect.

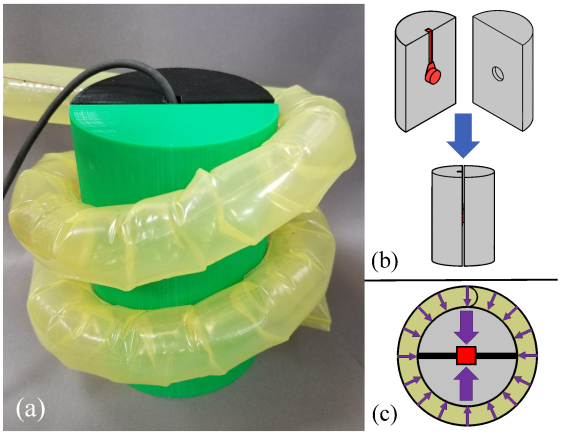

Fig. 8. Test set-up with instrumented cylinder to measure axial forces when deforming natural shape. a) Photograph of the instrumented cylinder assembly with soft robot wrapped around it in a helix. b) View of instrumented cylinder. The two half-cylinders each have recessions allowing for the placement of the F/T sensor shown in red. The two halves can be fit together to form a single cylinder with the F/T sensor located in the middle. c) Top view of forces on cylinder shown in purple. The cylinder converts radial forces into linear compressive forces that can be measured by the sensor. Only the components of the distributed forces normal to the sensor are measured.

The start and end conditions for the curves are indicated by filled circles. For R_o, all the curves start and end at the same point, while b curves start separately and end at a single point. At a $\lambda = 1$, the start point for R_o is the radius of the tube and the b curve will be at the pitch parameter of the actuator, since on the un-actuated tube the outer line will be a helix on the surface of the tube, as described in Section II-A.1. On the other extreme, though a $\lambda = 0$ is not actually realizable, we can think of this situation as collapsing the actuator line to a single point, which will result in a torus with an inner radius of zero. So the curves will end at a pitch, b, of zero and an outer radius, R_o, equal to the tube diameter.

C. Applied Forces

While actuation into a helical shape alone is advantageous for a variety of tasks, many applications will require the soft robot to apply forces as well. Helical climbing is used by a variety of snake-like robots to climb external structures, a behavior that can be leveraged to support a navigating robot or a deploying structure. Secure helical grasps will be dependent on the forces that can be applied [22]. We describe the experimental setup for finding the relationship between the helical shape and the applied forces to characterize these "grasping" behaviors and present the experimental results.

1) Experimental Procedures: An instrumented cylinder with a diameter of 4.0 cm and a height of 12 cm was used to investigate the grasping forces of a helical shaped soft robot (Fig. 8). The instrumented cylinder is composed of two 3-D printed half-cylinders made of acrylonitrile butadiene styrene (ABS). These two half-cylinders are separated from each other by a gap of 3 mm and joined by a 6-axis force/torque sensor (ATI Nano-17), which is lightly pressed into the half-cylinders. The sensor has a range of 12 N and a resolution of 0.3 mN. The gap between the two half-cylinders ensures that the normal components of the radial compressive forces are transmitted between the two halves solely through the 6-axis force/torque sensor (Fig. 8c).

The soft actuators used for these tests were mechanically programmed, as described in Section III-A.1, to each have a pitch of 8.0 cm and were constructed in the same manner. Since we only expect grasp forces when the grasper radius is smaller than the object radius, radii less than or equal to 4.0 cm were tested. Radii deflections, ΔR_i, equal to 0, 2, and 4 mm were tested. During the tests, 1.5 revolutions of the robot were wrapped around the instrumented cylinder. Pressure was measured by an analog pressure gauge (NXP MPX5100) read through an Arduino Uno, and was manually incremented throughout the test.

2) Test Results: As seen in Fig. 9, there is a linear relationship between pressure and force, with the average R^2 value of 0.958. Additionally, a larger ΔR_i results in an increase in the magnitude of the radial compressive forces recorded.

The linear trend between grasping force and pressure can be understood through an argument from virtual work. By imagining a virtual contraction between the two halves of the cylinder as shown in Fig. 8c, we can relate the work done by the measured force F over the distance of a virtual contraction dL to the work done by the pressure P due to a volume change dV, i.e. $FdL = PdV$. Solving for force we get:

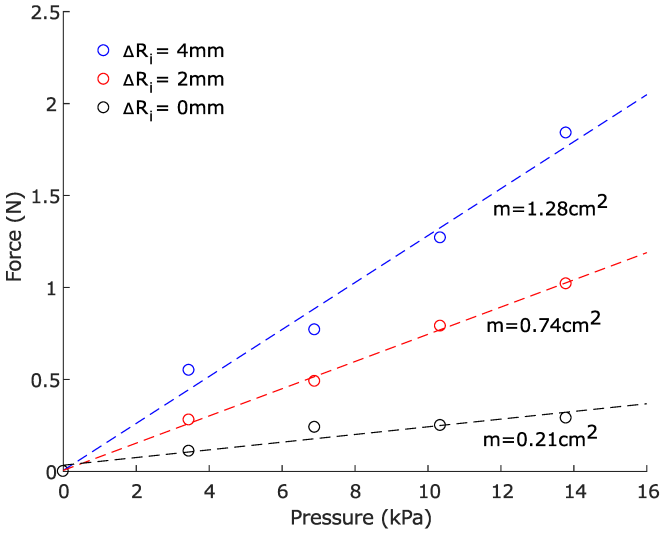

Fig. 9. The relationship between the compressive force between the two halves of the instrumented cylinder and pressure for three different robots and resulting force to deform soft robot.

$$F = P\frac{dV}{dL} \tag{18}$$

Because $\frac{dV}{dL}$ is a geometric term and the cylinder size constrains the robot geometry, for a fixed cylinder size the force will increase linearly with pressure, as seen in Fig. 9. For larger ΔR_i the $\frac{dV}{dL}$ term is larger, leading to higher forces at the same pressures.

This virtual work argument does imply that a ΔR_i equal to 0 mm will apply zero force. However, the instrumented object was slightly elliptical in cross-section due to the gap between the half-cylinders, so this actuator was still deflected by the instrumented object.

IV. Conclusion

In summary, we have developed a static kinematic model for inflated soft robots using a geometric approach. The model parameterizes the helical actuator and resultant shape and develops the geometric constraints necessary to relate the two parameterizations. The helical actuation is implemented, validated and some initial deformation responses are investigated. In this work we assumed the resulting shapes were uniform helices and just measure the pitch and radius parameters. Measuring the entire shape of the resulting robot will further validate the shape and uniformity of the actuated helices. The grasping force results show promise for using helical body grasping. Future work will model these grasping strategies with soft robot bodies.

This geometric model facilitates the design of actuators to achieve desired helical shapes for deployable antennas and soft body grasping. In the future, the model can be extended to investigate more general shape actuation of inflated soft robots by allowing the actuator parameters to vary along the length. This will be supported by developing actuators that can achieve these more general actuations.

References

[1] D. Rus and M. T. Tolley, "Design, fabrication and control of soft robots," *Nature*, vol. 521, no. 7553, pp. 467–475, 2015.

[2] J. Bishop-Moser and S. Kota, "Design and modeling of generalized fiber-reinforced pneumatic soft actuators," *IEEE Transactions on Robotics*, vol. 31, no. 3, pp. 536–545, 2015.

[3] P. Polygerinos, S. Lyne, Z. Wang, L. F. Nicolini, B. Mosadegh, G. M. Whitesides, and C. J. Walsh, "Towards a soft pneumatic glove for hand rehabilitation," in *IEEE/RSJ International Conference on Intelligent Robots and Systems*. IEEE, 2013, pp. 1512–1517.

[4] F. Connolly, P. Polygerinos, C. J. Walsh, and K. Bertoldi, "Mechanical programming of soft actuators by varying fiber angle," *Soft Robotics*, vol. 2, no. 1, pp. 26–32, 2015.

[5] M. D. Gilbertson, G. McDonald, G. Korinek, J. D. V. de Ven, and T. M. Kowalewski, "Serially actuated locomotion for soft robots in tube-like environments," *IEEE Robotics and Automation Letters*, vol. 2, no. 2, pp. 1140–1147, 2017.

[6] R. J. Webster III and B. A. Jones, "Design and kinematic modeling of constant curvature continuum robots: A review," *The International Journal of Robotics Research*, vol. 29, no. 13, pp. 1661–1683, 2010.

[7] J. Starke, E. Amanov, M. T. Chikhaoui, and J. Burgner-Kahrs, "On the merits of helical tendon routing in continuum robots," in *IEEE/RSJ International Conference on Intelligent Robots and Systems*, 2017, pp. 6470–6476.

[8] G. Gerboni, P. W. Henselmans, E. A. Arkenbout, W. R. van Furth, and P. Breedveld, "Helixflex: bioinspired maneuverable instrument for skull base surgery," *Bioinspiration & biomimetics*, vol. 10, no. 6, p. 066013, 2015.

[9] E. W. Hawkes, L. H. Blumenschein, J. D. Greer, and A. M. Okamura, "A soft robot that navigates its environment through growth," *Science Robotics*, vol. 2, no. 8, p. eaan3028, 2017.

[10] L. H. Blumenschein, A. M. Okamura, and E. W. Hawkes, "Modeling of bioinspired apical extension in a soft robot," in *Conference on Biomimetic and Biohybrid Systems*. Springer, 2017, pp. 522–531.

[11] L. H. Blumenschein, L. Gan, J. Fan, A. M. Okamura, and E. W. Hawkes, "A tip-extending soft robot enables reconfigurable and deployable antennas," *IEEE Robotics and Automation Letters*, vol. 3, no. 2, pp. 949–956, 2018.

[12] S. Neppalli, B. Jones, W. McMahan, V. Chitrakaran, I. Walker, M. Pritts, M. Csencsits, C. Rahn, and M. Grissom, "Octarm-a soft robotic manipulator," in *IEEE/RSJ International Conference on Intelligent Robots and Systems*, 2007, pp. 2569–2569.

[13] D. Trivedi, C. D. Rahn, W. M. Kier, and I. D. Walker, "Soft robotics: Biological inspiration, state of the art, and future research," *Applied Bionics and Biomechanics*, vol. 5, no. 3, pp. 99–117, 2008.

[14] J. Costantine, Y. Tawk, S. E. Barbin, and C. G. Christodoulou, "Reconfigurable Antennas: Design and Applications," *Proceedings of the IEEE*, vol. 103, no. 3, pp. 424–437, 2015.

[15] K. Lipkin, I. Brown, A. Peck, H. Choset, J. Rembisz, P. Gianfortoni, and A. Naaktgeboren, "Differentiable and piecewise differentiable gaits for snake robots," in *IEEE/RSJ International Conference on Intelligent Robots and Systems*, 2007, pp. 1864–1869.

[16] D. C. Rucker and R. J. Webster III, "Statics and dynamics of continuum robots with general tendon routing and external loading," *IEEE Transactions on Robotics*, vol. 27, no. 6, pp. 1033–1044, 2011.

[17] I. D. Walker, "The importance of torsion in robot backbones," in *Recent Advances in Circuits, Systems, Signal Processing and Communications*. World Scientific and Engineering Academy and Society (WSEAS), 2014, pp. 25–31.

[18] E. W. Hawkes, D. L. Christensen, and A. M. Okamura, "Design and implementation of a 300% strain soft artificial muscle," pp. 4022–4029, 2016.

[19] M. Kaneko, T. Yamashita, and K. Tanie, "Basic considerations on transmission characteristics for tendon drive robots," in *Fifth International Conference on Advanced Robotics, 'Robots in Unstructured Environments'*. IEEE, 1991, pp. 827–832.

[20] C.-P. Chou and B. Hannaford, "Measurement and modeling of mckibben pneumatic artificial muscles," *IEEE Transactions on Robotics and Automation*, vol. 12, no. 1, pp. 90–102, 1996.

[21] J. D. Greer, T. K. Morimoto, A. M. Okamura, and E. W. Hawkes, "Series pneumatic artificial muscles (sPAMs) and application to a soft continuum robot," pp. 5503–5510, 2017.

[22] W. S. Howard and V. Kumar, "On the stability of grasped objects," *IEEE Transactions on Robotics and Automation*, vol. 12, no. 6, pp. 904–917, 1996.